IEEE Access
Multidisciplinary | Rapid Review | Open Access Journal

Received 29 December 2023, accepted 26 January 2024, date of publication 30 January 2024, date of current version 7 February 2024.

Digital Object Identifier 10.1109/ACCESS.2024.3360333

RESEARCH ARTICLE

Robust Feedback Linearization Based Disturbance Observer Control of Quadrotor UAV

MOHAMMAD SADIQ[1], RAMEEZ HAYAT[1], KAMRAN ZEB[2], AHMED AL-DURRA[3], (Senior Member, IEEE), AND ZAHID ULLAH[4], (Graduate Student Member, IEEE)

[1]School of Electrical Engineering and Computer Science (SEECS), National University of Sciences and Technology (NUST), Islamabad 44000, Pakistan
[2]Interdisciplinary Research Center for Sustainable Energy Systems, King Fahd University of Petroleum and Minerals (KFUPM), Dhahran 31261, Saudi Arabia
[3]Advanced Power and Energy Center, Department of Electrical Engineering and Computer Science, Khalifa University, Abu Dhabi, United Arab Emirates
[4]Dipartimento di Elettronica, Informazione e Bioingegneria, Politecnico di Milano, 20133 Milan, Italy

Corresponding author: Zahid Ullah (zahid.ullah@polimi.it)

This work was supported in part by the National University of Sciences and Technology funded by ICT Endowment Scholarship, and in part by Politecnico di Milano for providing Open Access within the CRUI CARE Agreement.

ABSTRACT This paper presents a novel Robust Feedback Linearization (RFBL) controller for Quadrotor Unmanned Aerial Vehicle (UAV) when subjected to external disturbances. A Robust Feedback Linearization controller is achieved by augmenting the conventional Feedback Linearization-based control with the Supertwisting Algorithm in the outer loop. To estimate the external disturbances acting on a quadrotor a Nonlinear Harmonic Disturbance Observer (NHDO) is patched with the robust controller. The efficacy and superiority of the results can be seen in terms of tracking error, rise time and robustness to disturbances when comparing it with other three robust controllers i.e. Integral Sliding Mode Controller (ISMC), Terminal Synergetic Controller (TSC) and Finite-Time supertwisting controller. Lyapunov's stability analysis is performed to prove stability while numerical simulation is carried out using MATLAB/Simulink. The results are also validated by testing the system in a Hardware-In-Loop (HIL) environment on the MicroLabBox dSPACE RTI-1202 platform.

INDEX TERMS Disturbance observer, quadrotor, robust feedback linearization control, supertwisting control.

I. INTRODUCTION

The application of drones for delivery purposes has shown an increasing popularity and is believed to be 90 % cheaper than car-based services [1]. Big companies such as Amazon and DHL have started delivery of parcels using drones which does not have the adverse effects that internal combustion engine vehicles do; such as congestion, noise and pollutant emissions [2]. Other uses of drones include infrastructure inspection, pesticide spraying on crops, army reconnaissance missions and target tracking [3]. Among the different types of Unmanned Aerial Vehicles (UAVs), quadrotors are the most popular since it can take off and land vertically compared to a fixed-wing aerial vehicle. Also it has high maneuverability and can lift heavy loads when compared to a helicopter. With such vast utilization, quadrotors need to be robust to external disturbances such as wind gusts, modelling and parametric uncertainties (due to varying payloads and inaccurate modelling of the quadrotor). Therefore robust control is required to compensate for these negative effects. A comprehensive survey can be found in [4], which discusses the vast types of controllers that have been implemented on a quadrotor-type UAV. It can be seen that sliding mode control has been the most investigated type of controller, however has the adverse effect of chattering. Moreover, a gap in the research literature for attitude based robust feedback linearization control is found. Since feedback linearization makes the system exactly linear, therefore controllers can easily be designed for it.

The literature survey can be split between attitude based and position based control of quadrotors. For the attitude based control, in [5], a nonlinear sliding surface has been

The associate editor coordinating the review of this manuscript and approving it for publication was Guillermo Valencia-Palomo.

© 2024 The Authors. This work is licensed under a Creative Commons Attribution 4.0 License.
For more information, see https://creativecommons.org/licenses/by/4.0/

chosen to construct a TSMC (Terminal Sliding Mode Controller) based controller along with an enhanced disturbance observer for mismatched disturbances. Only regulation of attitude has been achieved. Even though TSMC is finite time convergent while enhanced DO (Disturbance Observer) has asymptotic convergence still the author has managed to use them together. The same author has managed to achieve an adaptive backstepping sliding mode controller patched with a disturbance observer along with state estimation in [6]. For state estimation a high-gain observer has been used. However, a relatively large settling time for the estimation of disturbance is noted. In another paper [7], tracking of attitude and altitude utilizing standard sliding mode control complemented with disturbance estimation for both matched and mismatched uncertainties using Simpson's approximation has been utilized. The disturbances are high order polynomials which are approximated and attenuated using the developed disturbance observer.

Quadcopter control for mismatched uncertainties based on nonlinear DO based on sliding mode control has been achieved in [8]. The Nonlinear DO exhibits the salient feature that requires the gains to be larger than the bound of error of the disturbance estimation than that of disturbance. Regulation of attitude has been achieved with the shortcoming of tracking of attitude reference. Moreover, the controller achieves finite-time convergence while the nonlinear DO has asymptotic convergence. A dynamic sliding mode control patched with a nonlinear disturbance observer has been implemented in [9]. Attitude regulation has been achieved and matched nonlinear disturbances has been estimated and attenuated. A dual fixed-time attitude control is investigated for a quadrotor unmanned aerial vehicle in [10]. To estimate the external disturbances a fixed-time adaptive fast supertwisting disturbance observer is used. For the controller part, a fixed-time controller is designed by using a universal barrier lyapunov function to achieve good tracking error constraints. A tracking differentiator is also used along in the process for appropriate references and its derivative.

A fault-tolerant controller is designed that can simultaneously cater for actuator faults, external disturbances and parametric uncertainties in [11]. An adaptive control methodology is employed in both the continuous and discontinuous control to accommodate actuator faults and parametric uncertainty. Then a nonlinear disturbance observer is integrated to reject the external disturbances and thereby keeping magnitude of the discontinuous control part small. The results are demonstrated through numerical simulations and experimental verification. A disturbance observer-based attitude control for aggressive maneuver has been implemented [12]. Cascade connection based controller is developed: for the outer attitude control loop a quaternion based controller is developed and disturbance observer based angular velocity control is for the inner loop.

In the following article [13] an optimization based framework for the nonlinear disturbance observer is developed. The optimization is based on infinity-norm minimization of noise-to-output transfer function along with the load disturbance sensitivity function. Step, square and sinusoidal disturbances are applied in hover and flying modes. The proposed work is verified through simulations and implemented on real-time embedded controller for experimental verification.

For the altitude and attitude control, a state-feedback linearization based controller along with arbitrary order differentiator for estimation and rejection of external disturbances has been implemented [14]. The results are verified on an experimental setup.

An enhanced extended state observer (ESO) is implemented to cater for wind gusts and actuator faults along with a supertwisting controller [15]. The extended state observer provides finite time stability whereas the supertwisting controller achieves asymptotic convergence. Quadrotor dynamics based on quaternion has been used. Finite time extended state observer along with non-singular fast terminal sliding mode as the controller is implemented to cater modeling uncertainties and external disturbances [16]. A tracking differentiator is also designed to obtain smooth references and their derivatives. Simulation and experimental results validate the efficacy of the controller.

As for the position control, [17] a Finite-Time Sliding-Mode Observer which is used for state as well as disturbance estimation is utilized. For the control part PID controller and a continuous sliding mode controller has been designed in combination that achieve exponential convergence. The observer and controller are implemented in real time on an experimental platform. A nonlinear controller based on Euler angles as virtual control inputs is designed in [18]. This technique eliminates separation of timescale that is assumed in a hierarchical control system. The controller is based on dynamic surface control method while disturbance observers are designed to estimate disturbances in the translation and rotational dynamics of the quadcopter. The results are validated using numerical simulations. The feedback linearization strategy is patched with a disturbance observer to make it robust [19]. The disturbance observer accommodates nonlinearities in the model by considering them as disturbances. Simulation results show good tracking in the presence of unmodelled dynamics, actuator failure and wind disturbances.

Reference [20] develops a finite-time supertwisting controller with a high-order finite time disturbance observer. Lyapunov Analysis is used to study overall system stability and provide finite time convergence. The proposed controller is compared with PID and continuous sliding mode control coupled with a finite time disturbance observer. The results are validated using an experimental setup. In [21] a backstepping-based controller is developed along with incorporating a disturbance observer thus providing tracking of error dynamics exponentially. The errors are proven ultimately bounded for time-varying disturbances. The results are verified through simulations.

A finite time disturbance observer along with a geometric controller has been developed in [22]. A simple structure for the geometric controller is chosen which ensure exponentially stable error dynamics after finite time convergence by the disturbance estimator. Simulations are done to show to verification of the results. Finite-time continuous multi-variable control algorithm is developed in [23], which is used to develop both controller and observer. The states and disturbances are estimated through the observer whose stability and finite-time convergence is proved using Lyapunov analysis. Numerical simulation is used to verify the results.

In [24] proposes a continuous non-singular terminal sliding mode controller along with a Finite time observer. The sliding motion is independent of the system's initial condition which is achieved by utilizing a full-order homogeneous terminal sliding surface. Stability Analysis is done using bi-limit homogeneous theory, Lyapunov theory and Input-to-State Stability. Both Processor in Loop and experimental results are done to verify the results. A second-order supertwisting controller along with a finite time observer for estimation of states and external disturbances is presented in [25]. The efficacy of the results are compared with an adaptive gain controller in both simulations and experimental validation. Among the earlier papers published [26] presents a continuous sliding mode controller along with a sliding mode disturbance observer to cater for modelling uncertainties, lateral wind gusts and actuator damage/failure. The results are verified through simulations. In [27] the nonlinear dynamic inversion controller is robustified using an uncertainty and disturbance estimator to cater for system nonlinearities, input couplings and wind disturbances. The uncertainty and disturbance estimator is based on the time delay disturbance observer concept. The effectiveness of the results is verified through Monte Carlo simulations and verified on experimental hardware.

In this paper, a novel RFBL is designed along with two other robust controllers i.e. ISMC and TSC. RFBL achieves results superior to all other controllers for most of the cases with smaller tracking errors and settling time. The controllers have been compared with the controller and disturbance observer designed in [20] for several different reference trajectories. The controllers used for comparison are considered for their robust qualities and ease of implementation on a real platform. To the best of the author's knowledge, harmonic nonlinear disturbance observer has not been implemented on a quadrotor along with a robust feedback linearization approach. The overall contributions of the paper are enlisted as follows:

- A novel RFBL Controller has been designed that achieves superior results to several compared robust controllers (ISMC and TSC).
- Results of RFBL Controller when compared with the existing controller of [20] via multiple performance indices is far more superior.
- Lyapunov stability analysis is assured for all the designed controllers.
- Validation has been done both in simulations and Hardware-In-Loop experiments.

The paper has been organized as follows: Section II presents the mathematical modelling of the quadrotor. Section III includes the design of the robust controllers and nonlinear disturbance observer. In Section IV the results of both the simulation and S-HIL are presented. Lastly in Section V the conclusion is given.

II. MATHEMATICAL MODEL OF QUADROTOR

This section discusses the mathematical modelling of a quadrotor which can be achieved via several techniques among which Newton-Euler and Euler-Lagrange are the most popular. Considering position control, the mathematical model of quadrotor can be represented as [28]:

$$\begin{aligned}
\ddot{z} &= (cos\phi \cos\theta)\frac{F_z}{m} - g - \xi_z\frac{\dot{z}}{m} + d_z \\
\ddot{\phi} &= \dot{\theta}\dot{\psi}\frac{(I_y - I_z)}{I_x} - \frac{I_r}{I_x}\dot{\theta}\bar{\omega} - \frac{\xi_\phi}{I_x}\dot{\phi} + \frac{1}{I_x}\tau_\phi + d_\phi \\
\ddot{\theta} &= \dot{\phi}\dot{\psi}\frac{(I_z - I_x)}{I_y} - \frac{I_r}{I_y}\dot{\psi}\bar{\omega} - \frac{\xi_\theta}{I_y}\dot{\theta} + \frac{1}{I_y}\tau_\theta + d_\theta \\
\ddot{\psi} &= \dot{\phi}\dot{\theta}\frac{(I_x - I_y)}{I_z} - \frac{\xi_\psi}{I_z}\dot{\psi} + \frac{1}{I_z}\tau_\psi + d_\psi \\
\ddot{x} &= (cos\phi sin\theta cos\psi + sin\phi sin\psi)\frac{F_z}{m} - \xi_x\frac{\dot{x}}{m} + d_x \\
\ddot{y} &= (cos\phi sin\theta sin\psi - sin\phi sin\psi)\frac{F_z}{m} - \xi_y\frac{\dot{y}}{m} + d_y
\end{aligned} \tag{1}$$

where m denotes the mass of the quadrotor; g is the acceleration due to gravity; I_x, I_y, I_z are the moment of inertia for each axis; $\xi_z, \xi_\phi, \xi_\theta$ and ξ_ψ are the aerodynamic damping coefficients; I_r the inertia of the rotor; $\bar{\omega} = \omega_4 + \omega_3 - \omega_2 - \omega_1$ represents the residual rotor angular disturbance; F_z the thrust in z direction; $\tau_\phi, \tau_\theta, \tau_\psi$ the respective input torques in the roll, pitch and yaw axis. The disturbances acting on the system are $d_z, d_\phi, d_\theta, d_\psi, d_x$ and d_y.

Converting the above eq. 1 in state-space form yields:

$$\begin{aligned}
\dot{x_1} &= x_2 \\
\dot{x_2} &= (\cos x_3 \cos x_5)\frac{F_z}{m} - g - \xi_z\frac{x_2}{m} + d_z \\
\dot{x_3} &= x_4 \\
\dot{x_4} &= x_6x_8\frac{(I_y - I_z)}{I_x} - \frac{I_r}{I_x}x_6\bar{\omega} - \frac{\xi_\phi}{I_x}x_4 + \frac{1}{I_x}\tau_\phi + d_\phi \\
\dot{x_5} &= x_6 \\
\dot{x_6} &= x_4x_8\frac{(I_z - I_x)}{I_y} - \frac{I_r}{I_y}x_4\bar{\omega} - \frac{\xi_\theta}{I_y}x_6 + \frac{1}{I_y}\tau_\theta + d_\theta \\
\dot{x_7} &= x_8 \\
\dot{x_8} &= x_4x_6\frac{(I_x - I_y)}{I_z} - \frac{\xi_\psi}{I_z}x_8 + \frac{1}{I_z}\tau_\psi + d_\psi \\
\dot{x_9} &= x_{10} \\
\dot{x_{10}} &= -\frac{\xi_x}{m}x_{10} + \frac{F_zF_x}{m} + d_x
\end{aligned}$$

$$\dot{x}_{11} = x_{12}$$
$$\dot{x}_{12} = -\frac{\xi_y}{m}x_{12} + \frac{F_z F_y}{m} + d_y \tag{2}$$

As seen from eq. 1, the quadrotor is an under-actuated system. To convert it into a fully actuated system, virtual control inputs F_x and F_y are introduced to control motion in the x,y axis.

The desired roll and pitch angles can then be represented as:

$$\left.\begin{aligned}\phi_{des} &= \tfrac{1}{F_z}(F_x sin\psi^d - F_y cos\psi^d)\\ \theta_{des} &= \tfrac{1}{F_z}(F_x cos\psi^d - F_y sin\psi^d)\end{aligned}\right\} \tag{3}$$

For a quadrotor in X-configuration the matrix relating the thrust force and torques with the speed of the propeller's can be written as:

$$\begin{pmatrix} F_z \\ \tau_\phi \\ \tau_\theta \\ \tau_\psi \end{pmatrix} = \begin{pmatrix} -k_F & -k_F & -k_F & -k_F \\ -\frac{1}{\sqrt{2}}lk_F & -\frac{1}{\sqrt{2}}lk_F & \frac{1}{\sqrt{2}}lk_F & \frac{1}{\sqrt{2}}lk_F \\ \frac{1}{\sqrt{2}}lk_F & -\frac{1}{\sqrt{2}}lk_F & -\frac{1}{\sqrt{2}}lk_F & \frac{1}{\sqrt{2}}lk_F \\ k_M & -k_M & k_M & -k_M \end{pmatrix} \begin{pmatrix} \Omega_1^2 \\ \Omega_2^2 \\ \Omega_3^2 \\ \Omega_4^2 \end{pmatrix} \tag{4}$$

where k_F and k_M represents the thrust coefficient, l the length of the arm of the quadrotor.

Rearranging the above equation 4, the required propeller's rotational speed can be represented as:

$$\begin{pmatrix} \Omega_1 \\ \Omega_2 \\ \Omega_3 \\ \Omega_4 \end{pmatrix} = \begin{pmatrix} -\frac{1}{4k_F} & -\frac{1}{2\sqrt{2}lk_F} & \frac{1}{2\sqrt{2}lk_F} & \frac{1}{4k_M} \\ -\frac{1}{4k_F} & -\frac{1}{2\sqrt{2}lk_F} & -\frac{1}{2\sqrt{2}lk_F} & -\frac{1}{4k_M} \\ -\frac{1}{4k_F} & \frac{1}{2\sqrt{2}lk_F} & -\frac{1}{2\sqrt{2}lk_F} & \frac{1}{4k_M} \\ -\frac{1}{4k_F} & \frac{1}{2\sqrt{2}lk_F} & \frac{1}{2\sqrt{2}lk_F} & -\frac{1}{4k_M} \end{pmatrix} \begin{pmatrix} F_z \\ \tau_\phi \\ \tau_\theta \\ \tau_\psi \end{pmatrix} \tag{5}$$

III. ROBUST CONTROL AND DISTURBANCE OBSERVER DESIGN

A. CONTROLLER DESIGN

To facilitate control system design, it will be divided into Altitude/Attitude Control and Position X-Y control.

FIGURE 1. X-configuration parrot mambo drone.

1) ALTITUDE AND ATTITUDE CONTROL

The mathematical model for the Altitude and Attitude control of a quadrotor without considering the disturbances can be written as:

$$\begin{aligned}
\dot{x_1} &= x_2 \\
\dot{x_2} &= (\cos x_3 \cos x_5)\frac{F_z}{m} - g - \xi_z\frac{x_2}{m} + d_z \\
\dot{x_3} &= x_4 \\
\dot{x_4} &= x_6 x_8 \frac{(I_y - I_z)}{I_x} - \frac{I_r}{I_x}x_6\bar{\omega} - \frac{\xi_\phi}{I_x}x_4 + \frac{1}{I_x}\tau_\phi + d_\phi \\
\dot{x_5} &= x_6 \\
\dot{x_6} &= x_4 x_8 \frac{(I_z - I_x)}{I_y} - \frac{I_r}{I_y}x_4\bar{\omega} - \frac{\xi_\theta}{I_y}x_6 + \frac{1}{I_y}\tau_\theta + d_\theta \\
\dot{x_7} &= x_8 \\
\dot{x_8} &= x_4 x_6 \frac{(I_x - I_y)}{I_z} - \frac{\xi_\psi}{I_z}x_8 + \frac{1}{I_z}\tau_\psi + d_\psi
\end{aligned} \tag{6}$$

representing the above eq. 6 in the form $\dot{x} = f(x) + g(x)u + d$, where $f(x)$, $g(x)$, u and d can be written as:

$$f(x) = \begin{bmatrix} x_2 \\ -g - \xi_z\frac{x_2}{m} \\ x_4 \\ x_6 x_8 \frac{(I_y - I_z)}{I_x} - \frac{I_r}{I_x}x_6\bar{\omega} - \frac{\xi_\phi}{I_x}x_4 \\ x_6 \\ x_4 x_8 \frac{(I_z - I_x)}{I_y} - \frac{I_r}{I_y}x_4\bar{\omega} - \frac{\xi_\theta}{I_y}x_6 \\ x_8 \\ x_4 x_6 \frac{(I_x - I_y)}{I_z} - \frac{\xi_\psi}{I_z}x_8 \end{bmatrix} \tag{7}$$

$$g(x) = \begin{bmatrix} 0 & 0 & 0 & 0 \\ \frac{\cos x_3 \cos x_5}{m} & 0 & 0 & 0 \\ 0 & 0 & 0 & 0 \\ 0 & \frac{1}{I_x} & 0 & 0 \\ 0 & 0 & 0 & 0 \\ 0 & 0 & \frac{1}{I_y} & 0 \\ 0 & 0 & 0 & 0 \\ 0 & 0 & 0 & \frac{1}{I_z} \end{bmatrix} \tag{8}$$

$$u = \begin{bmatrix} F_z \\ \tau_\phi \\ \tau_\theta \\ \tau_\psi \end{bmatrix} \tag{9}$$

$$d = \begin{bmatrix} 0 \\ d_z \\ 0 \\ d_\phi \\ 0 \\ d_\theta \\ 0 \\ d_\psi \end{bmatrix} \tag{10}$$

Inorder to implement input-to-state feedback linearization, the control action can be calculated as:

$$\begin{bmatrix} F_z \\ \tau_\phi \\ \tau_\theta \\ \tau_\psi \end{bmatrix} = \begin{bmatrix} \frac{m}{\cos x_3 \cos x_5}(g + \xi_z \frac{x_2}{m} + v_1 - \hat{d}_z) \\ I_x(-x_6 x_8 \frac{(I_y - I_z)}{I_x} + \frac{I_r}{I_x} x_6 \bar{\omega} + \frac{\xi_\phi}{I_x} x_4 + v_2 - \hat{d}_\phi) \\ I_y(-x_4 x_8 \frac{(I_z - I_x)}{I_y} + \frac{I_r}{I_y} x_4 \bar{\omega} + \frac{\xi_\theta}{I_y} x_6 + v_3 - \hat{d}_\theta) \\ I_z(-x_4 x_6 \frac{(I_x - I_y)}{I_z} + \frac{\xi_\psi}{I_z} x_8 + v_4 - \hat{d}_\psi) \end{bmatrix} \tag{11}$$

where $\hat{d}_z, \hat{d}_\phi, \hat{d}_\theta$ and $\hat{d}_\psi$ are the estimated disturbances. Considering tracking problem, the inputs a proportional derivative controller can be designed as v_1, v_2, v_3 and v_4, which are the control inputs to the feedback linearized plant:

$$\left.\begin{aligned} v_1 &= \dot{x}_2^d - K_{pz} e_1 - K_{dz} e_2 \\ v_2 &= \dot{x}_4^d - K_{p\phi} e_3 - K_{d\phi} e_4 \\ v_3 &= \dot{x}_6^d - K_{p\theta} e_5 - K_{d\theta} e_6 \\ v_4 &= \dot{x}_8^d - K_{p\psi} e_7 - K_{d\psi} e_8 \end{aligned}\right\} \tag{12}$$

where $e_i = x_i - x_i^d$, where $i = 1, \ldots, 8$ and x_i^d is the desired state trajectory.

In-order to add robustness to the existing controller, a supertwisting controller will be added in the outer-loop of the feedback linearized controller. Addition of the supertwisting control action modifies the control inputs v_1, v_2, v_3 and v_4 as:

$$\left.\begin{aligned} v_{1,new} &= \dot{x}_2^d - K_{pz} e_1 - K_{dz} e_2 - k_{1z} |s_z|^{0.5} sign(s_z) \\ &\quad -k_{2z} \int sign(s_z)\, dt \\ v_{2,new} &= \dot{x}_4^d - K_{p\phi} e_3 - K_{d\phi} e_4 - k_{1\phi} |s_\phi|^{0.5} sign(s_\phi) \\ &\quad -k_{2\phi} \int sign(s_\phi)\, dt \\ v_{3,new} &= \dot{x}_6^d - K_{p\theta} e_5 - K_{d\theta} e_6 - k_{1\theta} |s_\theta|^{0.5} sign(s_\theta) \\ &\quad -k_{2\theta} \int sign(s_\theta)\, dt \\ v_{4,new} &= \dot{x}_8^d - K_{p\psi} e_7 - K_{d\psi} e_8 - k_{1\psi} |s_\psi|^{0.5} sign(s\psi) \\ &\quad -k_{2\psi} \int sign(s_\psi)\, dt \end{aligned}\right\} \tag{13}$$

where k_1 and k_2 are the gains of the supertwisting controller for the z-direction, roll, pitch and yaw-axis. The sliding surface for the supertwisting controller can be represented as:

$$\left.\begin{aligned} s_z &= c_1 e_1 + e_2 \\ s_\phi &= c_2 e_3 + e_4 \\ s_\theta &= c_3 e_5 + e_6 \\ s_\psi &= c_4 e_7 + e_8 \end{aligned}\right\} \tag{14}$$

where c_1, c_2, c_3, c_4 are the design constants.

2) STABILITY ANALYSIS OF ALTITUDE AND ATTITUDE CONTROLLER

First analyzing the stability of the feedback linearization based controller part, the system can be written in the following standard form, $\dot{e} = A_{cl}\ e$, where A_{cl} is the closed loop error dynamics matrix represented as: (15), as shown at the bottom of the next page.

The stability of the closed-loop system is ensured by selecting values of $K_p, K_d > 0$, which yields $eig|A_{cl}| < 0$. This ensures that the errors $e_i \to 0$ as $t \to \infty$, where $i = 1, \ldots, 8$.

As for the supertwisting controller, the stability can be derived from [29] as:

$$\left.\begin{aligned} \dot{z_1} &= -k_1 |z_1|^{0.5} sign(z_1) + z_2 \\ \dot{z_2} &= -k_2 sign(z_2) + \rho \end{aligned}\right\} \tag{16}$$

where $z_1, z_2 \in \mathbb{R}$ and the disturbance ρ is bounded by $|z_1| < \delta$.

Consider a lyapunov function which can be written in quadratic form as $V_1 = \zeta^T P\ \zeta$ where $\zeta^T = \begin{bmatrix} |z_1|^{0.5} sign(z_1) & z_2 \end{bmatrix}$ and P is positive definite matrix. V_1 is continuously differentiable except for when $z_1 = 0$. $\dot{V}_1$ exists and is negative differentiable $\forall z_1 \neq 0$.

The Lyapunov function V_1 is both positive definite and radially unbounded:

$$\lambda_{min}(P) \|\zeta\|^2 \leq V_1 \leq \lambda_{max}(P) \|\zeta\|^2 \tag{17}$$

The Euclidean norm of ζ can be written as $\|\zeta\|_2^2 = |z_1| + z_2^2$. The following algebraic equation can be constructed:

$$\begin{pmatrix} A^T P + PA + \epsilon P + \delta^2 C^T C & PB \\ B^T P & -1 \end{pmatrix} < 0 \tag{18}$$

where $A = \begin{bmatrix} -\frac{1}{2}k_1 & \frac{1}{2} \\ -k_2 & 0 \end{bmatrix}; B = \begin{bmatrix} 0 \\ 1 \end{bmatrix}$ and $C = \begin{bmatrix} 0 & 1 \end{bmatrix}$, with $k_1, k_2 > 0$. Using $\zeta^T = \begin{bmatrix} |z_1|^{0.5} sign(z_1) & z_2 \end{bmatrix}$, eq. 16 can be written as:

$$\dot{\zeta_1} = \frac{1}{|\zeta_1|}(A\zeta + B\tilde{\rho}) \tag{19}$$

Using the assumption that the perturbation is uniformly bounded satisfying $2|\rho| \leq \delta$, the transformed perturbation $\tilde{\rho} = |\zeta_1| \rho$ satisfies $|\tilde{\rho}| \leq \delta |\zeta_1|$. This results in $\hat{\omega} = -\tilde{\rho}^2 + \delta^2 \zeta_1^2 \geq 0$.

Considering the lyapunov equation $V_1 = \zeta^T P\ \zeta$, its derivative becomes:

$$\dot{V}_1 = \frac{1}{|\zeta_1|} [\zeta \quad \tilde{\rho}]^T \begin{bmatrix} A^T P + PA & PB \\ B^T P & -1 \end{bmatrix} [\zeta \quad \tilde{\rho}]$$

$$\leq \frac{1}{|\zeta_1|}\left\{[\zeta \quad \tilde{\rho}]^T \begin{bmatrix} A^TP+PA & PB \\ B^TP & -1 \end{bmatrix}[\zeta \quad \tilde{\rho}] + \hat{\omega}\right\}$$
$$\leq \frac{1}{|\zeta_1|}[\zeta \quad \tilde{\rho}]^T \begin{bmatrix} A^TP+PA+\delta^2C^TC & PB \\ B^TP & -1 \end{bmatrix}[\zeta \quad \tilde{\rho}]$$
$$\leq \frac{1}{|\zeta_1|}[\zeta \ \tilde{\rho}]^T \begin{bmatrix} A^TP+PA+\epsilon P-\epsilon P+\delta^2C^TC & PB \\ B^TP & -1 \end{bmatrix}[\zeta \ \tilde{\rho}]$$
$$\leq -\frac{\epsilon}{|\zeta_1|}\zeta^T P\,\zeta \tag{20}$$

Therefore $\dot{V}_1 \leq -\frac{\epsilon}{|\zeta_1|}\zeta^T P\,\zeta = -\frac{\epsilon}{|\zeta_1|}V_1$.

From the eq. 17 the following inequality can be deduced: $|\zeta_1| \leq \|\zeta\| \leq \frac{V_1^{0.5}}{\lambda_{min}(P)}$.

This concludes that $\dot{V}_1$ satisfies $\dot{V}_1 \leq -\alpha V_1^{0.5}$, where $\alpha = \epsilon\lambda_{min}^{0.5}P$. This guarantees finite time convergence where time is bounded by $T_s = \frac{2V_1^{0.5}\zeta(0)}{\alpha}$, where $\zeta(0)$ is the initial value of ζ.

For the LMI equation in eq. 18 to be satisfied, the transfer function $G(s) = C(sI - A)^{-1}B$ has to satisfy the following $max_{\omega}\,|G(j\omega)| < 1$. This implies that $max_{\omega}\,|G(j\omega)| < \frac{1}{\delta}$.

Using this inequality the following conditions on the gains can be achieved $max_{\omega}\,|G(j\omega)| < \frac{1}{k}$ if $k_1^2 > k_2$. Then the conditions on k_1 and k_2 can be deduced as: $k_2 > \delta$ and $k_1^2 > 4k_2$.

3) POSITION X-Y CONTROLLER

The remaining part of the quadrotor dynamics can be represented as:

$$\left.\begin{aligned} \dot{x}_9 &= x_{10} \\ \dot{x}_{10} &= -\tfrac{\xi_x}{m}x_{10} + \tfrac{F_zF_x}{m} + d_x \\ \dot{x}_{11} &= x_{12} \\ \dot{x}_{12} &= -\tfrac{\xi_y}{m}x_{12} + \tfrac{F_zF_y}{m} + d_y \end{aligned}\right\} \tag{21}$$

The control action similar to the fully actuated system can be designed as:

$$\left.\begin{aligned} F_x &= \tfrac{m}{F_z}(\dot{x}_{10}^d + \tfrac{\xi_x}{m}x_{10} - K_{px}e_9 - K_{dx}e_{10} \\ &-k_{1x}\,|s_x|^{0.5}\,sign(s_x) - k_{2x}\textstyle\int sign(s_x) - \hat{d}_x) \\ F_y &= \tfrac{m}{F_z}(\dot{x}_{12}^d + \tfrac{\xi_y}{m}x_{12} - K_{py}e_{11} - K_{dy}e_{12} \\ &-k_{1y}\,|s_y|^{0.5}\,sign(s_y) - k_{2y}\textstyle\int sign(s_y) - \hat{d}_y) \end{aligned}\right\} \tag{22}$$

where $K_p, K_d > 0$ and k_1, k_2 are the controller design gains of the supertwisting controller, $e_i = x_i - x_i^d$, where $i = 9, \ldots, 12$ and x_i^d is the desired state trajectory. The sliding surfaces are chosen as:

$$\left.\begin{aligned} s_x &= c_5e_9 + e_{10} \\ s_y &= c_6e_{11} + e_{12} \end{aligned}\right\} \tag{23}$$

where c_5, c_6 are design constants of the sliding surface. The stability analysis for the X-Y position control can be performed similarly to the Altitude and Attitude Control stability analysis; by analyzing the proportional derivative controller and supertwisting controller separately assuming the thrust, F_z to be bounded.

B. NONLINEAR HARMONIC DISTURBANCE OBSERVER

A nonlinear harmonic disturbance observer can be implemented where the frequency of the disturbance in known but with unknown amplitude and phase. An enhanced formulation is presented where the requirement of the derivative of the state can be eluded.

The enhanced formulation of this harmonic disturbance observer is defined as [30]:

$$\begin{aligned} \dot{z} &= [A - l(x)g_2(x)C]z + Ap(x) \\ &\quad - l(x)[g_2(x)Cp(x) + f(x) + g_1(x)u] \end{aligned} \tag{24}$$

$$\left.\begin{aligned} \hat{\xi} &= z + p(x) \\ \hat{d} &= C\hat{\xi} \\ l(x) &= \tfrac{\partial p(x)}{\partial x} \end{aligned}\right\} \tag{25}$$

$$\dot{x} = f(x) + g_1(x)u + g_2(x)d \tag{26}$$

The error dynamics of the disturbance and its estimation is represented as:

$$\left.\begin{aligned} e_\xi &= \hat{\xi} - \xi \\ \dot{e_\xi} &= \dot{\hat{\xi}} - \dot{\xi} \\ &= \dot{z} + \tfrac{\partial p(x)}{\partial x}\dot{x} - A\xi \\ &= [A - l(x)g_2(x)C]z + Ap(x) \\ &-l(x)[g_2(x)Cp(x) + f(x) + g_1(x)u] \\ &+l(x)[f(x) + g_1(x)u + g_2(x)d] - A\xi \\ &= [A - l(x)g_2(x)C](\hat{\xi} - p(x)) + Ap(x) \\ &-l(x)[g_2(x)Cp(x) + f(x) + g_1(x)u] \\ &+l(x)[f(x) + g_1(x)u + g_2(x)C\xi] - A\xi \\ &= [A - l(x)g_2(x)C](\hat{\xi} - \xi) \\ &= [A - l(x)g_2(x)C]e_\xi \end{aligned}\right\} \tag{27}$$

From eq. 27 if $l(x)$ is selected such that $\hat{\xi}$ approaches ξ exponentially and $\dot{e_\xi}$ is globally exponentially stable.

$$A_{cl} = \begin{bmatrix} 0 & 1 & 0 & 0 & 0 & 0 & 0 & 0 \\ -K_{pz} & -K_{dz} & 0 & 0 & 0 & 0 & 0 & 0 \\ 0 & 0 & 0 & 1 & 0 & 0 & 0 & 0 \\ 0 & 0 & -K_{p\phi} & -K_{d\phi} & 0 & 0 & 0 & 0 \\ 0 & 0 & 0 & 0 & 0 & 1 & 0 & 0 \\ 0 & 0 & 0 & 0 & -K_{p\theta} & -K_{d\theta} & 0 & 0 \\ 0 & 0 & 0 & 0 & 0 & 0 & 0 & 1 \\ 0 & 0 & 0 & 0 & 0 & 0 & -K_{p\psi} & -K_{d\psi} \end{bmatrix} \tag{15}$$

The block diagram of this harmonic nonlinear disturbance observer is depicted in the figure below:

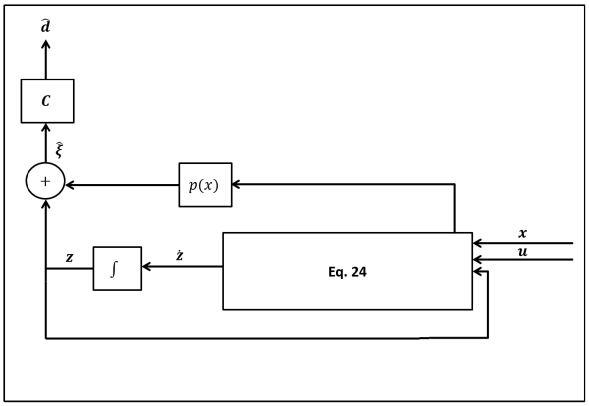

FIGURE 2. Block diagram of harmonic nonlinear disturbance observer.

Considering the quadrotor mathematical model with disturbances included as in eq. 2, the controller already designed can be patched with the estimates of the unmatched disturbances d_z, d_ϕ, d_θ, d_ψ, d_x and d_y.

The control action after the addition of estimated disturbance for the Altitude and Attitude system can be written as:

$$\left.\begin{aligned} v_{1,new} &= \dot{x}_2^d - K_{pz}e_1 - K_{dz}e_2 \\ &\quad -k_{1z}\left|s_z\right|^{0.5} sign(s_z) - k_{2z}\int sign(s_z)\,dt - \hat{d}_z \\ v_{2,new} &= \dot{x}_4^d - K_{p\phi}e_3 - K_{d\phi}e_4 \\ &\quad -k_{1\phi}\left|s_\phi\right|^{0.5} sign(s_\phi) - k_{2\phi}\int sign(s_\phi)\,dt - \hat{d}_\phi \\ v_{3,new} &= \dot{x}_6^d - K_{p\theta}e_5 - K_{d\theta}e_6 \\ &\quad -k_{1\theta}\left|s_\theta\right|^{0.5} sign(s_\theta) - k_{2\theta}\int sign(s_\theta)\,dt - \hat{d}_\theta \\ v_{4,new} &= \dot{x}_8^d - K_{p\psi}e_7 - K_{d\psi}e_8 \\ &\quad -k_{1\psi}\left|s_\psi\right|^{0.5} sign(s\psi) - k_{2\psi}\int sign(s_\psi) - \hat{d}_\psi \end{aligned}\right\} \tag{28}$$

while for the position X-Y system can be written as:

$$\left.\begin{aligned} F_x &= \tfrac{m}{F_z}(\dot{x}_{10}^d + \tfrac{\xi_x}{m}x_{10} - K_{px}e_9 - K_{dx}e_{10} \\ &\quad -k_{1x}\left|s_x\right|^{0.5} sign(s_x) - k_{2x}\int sign(s_x)\,dt - \hat{d}_x) \\ F_y &= \tfrac{m}{F_z}(\dot{x}_{12}^d + \tfrac{\xi_y}{m}x_{12} - K_{py}e_{11} - K_{dy}e_{12} \\ &\quad -k_{1y}\left|s_y\right|^{0.5} sign(s_y) - k_{2y}\int sign(s_y)\,dt - \hat{d}_y) \end{aligned}\right\} \tag{29}$$

C. INTEGRAL SLIDING MODE CONTROL

Integral Sliding Mode Control defers from the regular sliding mode controller by designing its sliding surface which includes the integral terms of all the errors [31].

1) CONTROLLER DESIGN

For Tracking of desired states, the sliding surface for the roll axis is defined as:

$$\left.\begin{aligned} s_\phi &= c_{1_\phi}e_{1_\phi} + e_{2_\phi} + c_{2_\phi}e_{3_\phi} + e_{4_\phi} \\ e_{1_\phi} &= x_3 - x_3^d \\ e_{2_\phi} &= x_4 - x_4^d \\ e_{3_\phi} &= \int(x_3 - x_3^d)dt \\ e_{4_\phi} &= \int(x_4 - x_4^d)dt \end{aligned}\right\} \tag{30}$$

The derivative of the sliding surface can be defined as:

$$\dot{s}_\phi = c_{1_\phi}\dot{e}_{1\phi} + \dot{e}_{2\phi} + c_{2_\phi}e_{1_\phi} + e_{2_\phi} \tag{31}$$

Inserting the time derivatives of the errors in eq. 31 yields:

$$\dot{s}_\phi = c_{1_\phi}(\dot{x}_3 - \dot{x}_3^d) + \dot{x}_4 - \dot{x}_4^d + c_{2_\phi}e_{1_\phi} + e_{2_\phi} \tag{32}$$

In order to make Lyapunov function negative-definite, we equate $\dot{s_\phi} = -k\left|s_\phi\right|^{0.5} sign(s_\phi)$.

The control action for the roll-axis then yields:

$$\begin{aligned} \tau_\phi = -I_x(\dot{x}_4^d + x_6x_8\frac{(I_y - I_z)}{I_x} - \frac{I_r}{I_x}x_6\bar{\omega} - \frac{\xi_\phi}{I_x}x_4 \\ + k_\phi\left|s_\phi\right|^{0.5} sign(s_\phi) + c_{1_\phi}e_{2_\phi} + c_{2_\phi}e_{1_\phi} + e_{2_\phi} - \hat{d}_\phi) \end{aligned} \tag{33}$$

where k_ϕ is the gain of the integral sliding mode and $\hat{d}_\phi$ is the estimated disturbance in the roll-axis.

The Integral Sliding Mode Controller for the x-axis can be designed as:

$$\begin{aligned} F_x = \frac{m}{F_z}(-\frac{\xi_x}{m}x_{10} - k_x\left|s_x\right|^{0.5} sign(s_x) \\ - c_{1x}e_{2x} - c_{2x}e_{1x} - e_{2x} - \hat{d}_x) \end{aligned} \tag{34}$$

where k_x is the gain of the integral sliding mode and $\hat{d}_x$ is the estimated disturbance in the x-axis.

The sliding surface is chosen as $s_x = c_{1x}e_{1_x} + e_{2_x} + c_{2x}e_{3_x} + e_{4_x}$,where c_{1x} and c_{2x} are the design parameter. The errors $e_{1_x} = x_9 - x_{9d}$, $e_{2_x} = x_{10} - x_{10d}$, $e_{3_x} = \int e_{1_x}\,dt$ and $e_{4_x} = \int e_{2_x}\,dt$.

The Integral Sliding Mode Control patched with harmonic disturbance observer for the complete quadrotor system for tracking of states is defined as:

$$\left.\begin{aligned} F_z &= \tfrac{m}{cosx_3cosx_5}(\dot{x}_2^d + g + \xi_z\tfrac{x_2}{m} - k_z\left|s_z\right|^{0.5} sign(s_z) \\ &\quad -c_{1z}x_2 - c_{2z}e_{1z} - e_{2z} - \hat{d}_z) \\ \tau_\phi &= I_x(\dot{x}_4^d - x_6x_8\tfrac{(I_y - I_z)}{I_x} + \tfrac{I_r}{I_x}x_6\bar{\omega} + \tfrac{\xi_\phi}{I_x}x_4 \\ &\quad -k_\phi\left|s_\phi\right|^{0.5} sign(s_\phi) - c_{1\phi}e_{2\phi} - c_{2\phi}e_{1\phi} - e_{2\phi} - \hat{d}_\phi) \\ \tau_\theta &= I_y(\dot{x}_6^d - x_4x_8\tfrac{(I_z - I_x)}{I_y} + \tfrac{I_r}{I_y}x_4\bar{\omega} + \tfrac{\xi_\theta}{I_y}x_6 \\ &\quad -k_\theta\left|s_\theta\right|^{0.5} sign(s_\theta) - c_{1\theta}e_{2\theta} - c_{2\theta}e_{1\theta} - e_{2\theta} - \hat{d}_\theta) \\ \tau_\psi &= I_z(\dot{x}_8^d - x_4x_6\tfrac{(I_x - I_y)}{I_z} + \tfrac{\xi_\psi}{I_z}x_8 \\ &\quad -k_\psi\left|s_\psi\right|^{0.5} sign(s_\psi) - c_{1\psi}e_{2\psi} - c_{2\psi}e_{1\psi} - e_{2\psi} - \hat{d}_\psi) \end{aligned}\right\} \tag{35}$$

while the control action for x and y axis can be defined as:

$$\left.\begin{aligned} F_x &= \tfrac{m}{F_z}(\dot{x}_{10}^d - \tfrac{\xi_x}{m}x_{10} - k_x\left|s_x\right|^{0.5} sign(s_x) \\ &\quad -c_{1x}e_{2x} - c_{2x}e_{1x} - e_{2x} - \hat{d}_x) \\ F_y &= \tfrac{m}{F_z}(\dot{x}_{12}^d - \tfrac{\xi_y}{m}x_{12} - k_y\left|s_y\right|^{0.5} sign(s_y) \\ &\quad -c_{1y}e_{2y} - c_{2y}e_{1y} - e_{2y} - \hat{d}_y) \end{aligned}\right\} \tag{36}$$

2) STABILITY ANALYSIS

Considering the Lyapunov candidate function as:

$$V = \frac{1}{2}s^2 \tag{37}$$

Taking its derivative we get $\dot{V} = s\dot{s}$. Inserting $\dot{s} = -k\,|s|^{0.5}\,sign(s)$, we get $\dot{V} = s(-k\,|s|^{0.5}\,sign(s))$.

For simplification $sign(s)$ can also be written as $sign(s) = \frac{|s|}{s}$. Substituting this in $\dot{V}$ gives:

$$\dot{V} = -k\,|s|^{1.5} \tag{38}$$

Since k is a positive number, $\dot{V}$ will always be negative definite, which ensures asymptotic stability.

D. TERMINAL SYNERGETIC CONTROLLER

Synergetic control achieves convergence of state variables as time goes to infinity [32]. To achieve finite time convergence Terminal Synergetic Control is used which combines synergetic control theory with terminal attractor to achieve finite time convergence.

1) CONTROLLER DESIGN

A controller for the roll-axis is developed, similarly controllers for the remaining axis can also be designed. We start by introducing a macro-variable ζ, which is expressed as:

$$\zeta = e_{1\phi} + w_{1\phi}(\int_0^t e_{1\phi}\,dt)^{p_1/q_1} + e_{2\phi} + w_{2\phi}(\int_0^t e_{2\phi}\,dt)^{p_2/q_2} \tag{39}$$

where $w_{1\phi}$ and $w_{2\phi}$ are positive constants chosen by the designer, while p_1,q_1,p_2 and q_2 are odd positive numbers such that $1 < \frac{p_1}{q_1} < 2$ and $1 < \frac{p_2}{q_2} < 2$. The errors are defined as $e_{1\phi} = x_3 - x_3^d$ and $e_{2\phi} = x_4 - x_4^d$.

Taking the time derivative of ζ we attain:

$$\begin{aligned}\dot{\zeta} = {} & \dot{e_{1\phi}} + w_{1\phi}(\frac{p_1}{q_1})e_{1\phi}(\int_0^t e_{1\phi}\,dt)^{p_1/q_1-1} + \dot{e_{2\phi}} \\ & + w_{2\phi}(\frac{p_2}{q_2})e_{2\phi}(\int_0^t e_{2\phi}\,dt)^{p_2/q_2-1}\end{aligned} \tag{40}$$

After placing the values of $\dot{e_1}$ and $\dot{e_2}$ we get:

$$\begin{aligned}\dot{\zeta} = {} & x_4 + w_{1\phi}(\frac{p_1}{q_1})e_{1\phi}(\int_0^t e_{1\phi}\,dt)^{p_1/q_1-1} + x_6x_8\frac{(I_y - I_z)}{I_x} \\ & - \frac{I_r}{I_x}x_6\bar{\omega} - \frac{\xi_\phi}{I_x}x_4 + \frac{1}{I_x}\tau_\phi - \dot{x}_4^d \\ & + w_{2\phi}(\frac{p_2}{q_2})e_{2\phi}(\int_0^t e_{2\phi}\,dt)^{p_2/q_2-1}\end{aligned} \tag{41}$$

Considering the following relation between ζ and $\dot{\zeta}$:

$$T_\phi\dot{\zeta} + \zeta = 0 \tag{42}$$

where T_ϕ is a positive constant and is the convergence rate of the terminal attractor.

By putting eq. 41 in eq. 42 we get:

$$\begin{aligned}& T_\phi(x_4 + w_{1\phi}(\frac{p_1}{q_1})e_{1\phi}(\int_0^t e_{1\phi}\,dt)^{p_1/q_1-1} + x_6x_8\frac{(I_y - I_z)}{I_x} \\ & - \frac{I_r}{I_x}x_6\bar{\omega} - \frac{\xi_\phi}{I_x}x_4 + \frac{1}{I_x}\tau_\phi \\ & - \dot{x}_4^d + w_{2\phi}(\frac{p_2}{q_2})e_{2\phi}(\int_0^t e_{2\phi}\,dt)^{p_2/q_2-1}) + \zeta = 0\end{aligned} \tag{43}$$

Solving eq. 43 for the control input τ_ϕ:

$$\begin{aligned}\tau_\phi = {} & I_x(\dot{x}_4^d - x_6x_8\frac{(I_y - I_z)}{I_x} + \frac{I_r}{I_x}x_6\bar{\omega} + \frac{\xi_\phi}{I_x}x_4 - \frac{\zeta_\phi}{T_\phi} - x_4 \\ & - w_{1\phi}(\frac{p_1}{q_1})e_{1\phi}(\int_0^t e_{1\phi}dt)^{p_1/q_1-1} \\ & - w_{2\phi}(\frac{p_2}{q_2})e_{2\phi}(\int_0^t e_{2\phi}dt)^{p_2/q_2-1})\end{aligned} \tag{44}$$

The Terminal Synergetic Controller for the x-axis position control is as follows:

$$\begin{aligned}F_x = {} & \frac{m}{F_z}(\dot{x}_{10}^d - \frac{\zeta_x}{T_x} - x_{10} - w_{1x}(\frac{p_1}{q_1})e_{1x}(\int_0^t e_{1x}\,dt)^{p_1/q_1-1} \\ & - w_{2x}(\frac{p_2}{q_2})e_{2x}(\int_0^t e_{2x}\,dt)^{p_2/q_2-1})\end{aligned} \tag{45}$$

where the macro-variable $\zeta_x = e_{1x} + w_{1x}(\int_0^t e_{1x}\,dt)^{p_1/q_1} + e_{2x} + w_{2x}(\int_0^t e_{2x}\,dt)^{p_2/q_2}$, the errors $e_{1x} = x_9 - x_9^d$, $e_{2x} = x_{10} - x_{10}^d$. w_{1x}, w_{2x} and T_x are the design constants.

TSC patched with harmonic disturbance observer for the complete quadrotor system for tracking of states is defined as:

$$\left.\begin{aligned}F_z = {} & \tfrac{m}{cosx_3cosx_5}(\dot{x}_2^d + g + \xi_z\tfrac{x_2}{m} - \tfrac{\zeta_x}{T_z} \\ & -x_2 - w_{1z}(\tfrac{p_1}{q_1})e_{1z}(\textstyle\int_0^t e_{1z}dt)^{p_1/q_1-1} \\ & -w_{2z}(\tfrac{p_2}{q_2})e_{2z}(\textstyle\int_0^t e_{2z}dt)^{p_2/q_2-1} - \hat{d}_z) \\ \tau_\phi = {} & I_x(\dot{x}_4^d - x_6x_8\tfrac{(I_y-I_z)}{I_x} + \tfrac{I_r}{I_x}x_6\bar{\omega} + \tfrac{\xi_\phi}{I_x}x_4 - \tfrac{\zeta_\phi}{T_\phi} \\ & -x_4 - w_{1\phi}(\tfrac{p_1}{q_1})e_{1\phi}(\textstyle\int_0^t e_{1\phi}dt)^{p_1/q_1-1} \\ & -w_{2\phi}(\tfrac{p_2}{q_2})e_{2\phi}(\textstyle\int_0^t e_{2\phi}dt)^{p_2/q_2-1} - \hat{d}_\phi) \\ \tau_\theta = {} & I_y(\dot{x}_6^d - x_4x_8\tfrac{(I_z-I_x)}{I_y} + \tfrac{I_r}{I_y}x_4\bar{\omega} + \tfrac{\xi_\theta}{I_y}x_6 - \tfrac{\zeta_\theta}{T_\theta} \\ & -x_6 - w_{1\theta}(\tfrac{p_1}{q_1})e_{1\theta}(\textstyle\int_0^t e_{1\theta}dt)^{p_1/q_1-1} \\ & -w_{2\theta}(\tfrac{p_2}{q_2})e_{2\theta}(\textstyle\int_0^t e_{2\theta}dt)^{p_2/q_2-1} - \hat{d}_\theta) \\ \tau_\psi = {} & I_z(\dot{x}_8^d - x_4x_6\tfrac{(I_x-I_y)}{I_z} + \tfrac{\xi_\psi}{I_z}x_8 - \tfrac{\zeta_\psi}{T_\psi} \\ & -x_8 - w_{1\psi}(\tfrac{p_1}{q_1})e_{1\psi}(\textstyle\int_0^t e_{1\psi}dt)^{p_1/q_1-1} \\ & -w_{2\psi}(\tfrac{p_2}{q_2})e_{2\psi}(\textstyle\int_0^t e_{2\psi}dt)^{p_2/q_2-1} - \hat{d}_\psi)\end{aligned}\right\} \tag{46}$$

while the control action for x and y axis can be defined as:

$$\left.\begin{aligned}F_x = {} & \tfrac{m}{F_z}(\dot{x}_{10}^d - \tfrac{\xi_x}{m}x_{10} - \tfrac{\zeta}{T_x} - x_{10} \\ & -w_{1x}(\tfrac{p_1}{q_1})e_{1x}(\textstyle\int_0^t e_{1x}\,dt)^{p_1/q_1-1} \\ & -w_{2x}(\tfrac{p_2}{q_2})e_{2x}(\textstyle\int_0^t e_{2x}\,dt)^{p_2/q_2-1} - \hat{d}_x) \\ F_y = {} & \tfrac{m}{F_z}(\dot{x}_{12}^d - \tfrac{\xi_y}{m}x_{12} - \tfrac{\zeta}{T_y} - x_{12} \\ & -w_{1y}(\tfrac{p_1}{q_1})e_{1y}(\textstyle\int_0^t e_{1y}\,dt)^{p_1/q_1-1} \\ & -w_{2y}(\tfrac{p_2}{q_2})e_{2y}(\textstyle\int_0^t e_{2y}\,dt)^{p_2/q_2-1} - \hat{d}_y)\end{aligned}\right\} \tag{47}$$

2) STABILITY ANALYSIS

The Lyapunov function can be considered as:

$$V_2 = \frac{1}{2}\zeta^2 \tag{48}$$

Taking the time derivative of eq. 45:

$$\dot{V}_2 = \zeta\dot{\zeta} \tag{49}$$

By equating value of $\dot{\zeta}$ from eq. 42 we get:

$$\dot{V}_2 = -\frac{\zeta^2}{T_2} \tag{50}$$

By putting in value of ζ^2 from eq. 45:

$$\dot{V}_2 = -\frac{2V_2}{T_2} \tag{51}$$

The solution of eq. 51 yields:

$$\dot{V}_2 = V_{02} e^{(-2/T_2)t} \tag{52}$$

where V_{02} is the value of the Lyapunov function at $t = 0$. Therefore eq. 52 ensures global exponential finite time stability.

IV. RESULTS

The numerical simulations have been carried out for the controllers designed i.e. RFBL Controller, ISMC and TSC. The three controllers have been patched with nonlinear harmonic disturbance observer. The results for all three controllers as well as the disturbance observer have been compared with that implemented in [20].

A. DISTURBANCE OBSERVER

Nonlinear Harmonic Disturbance Observer in comparison with Finite Time Disturbance Observer implemented in [20] will be presented in this section. It can be seen from the figures below that the nonlinear harmonic disturbance observer estimates disturbances much superior to that of [20].

The reference disturbance acting on each axis is $d_z, d_\phi, d_\theta, d_\psi, d_x, d_y = 0.1 \sin(2t)$.

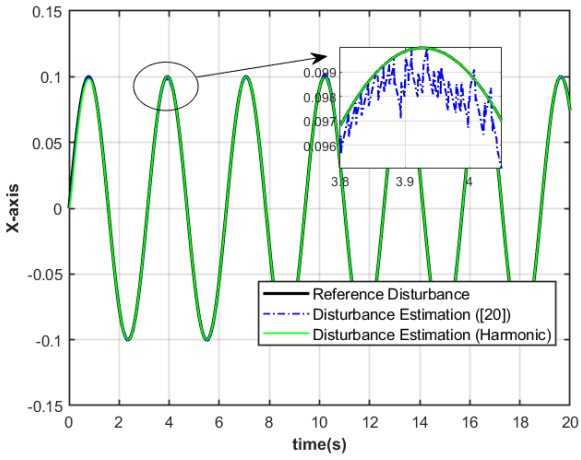

FIGURE 3. X-axis disturbance estimation.

B. CONTROLLER IMPLEMENTATION ON MULTIPLE TYPE OF TRAJECTORIES

In this section RFBL Controller designed will be compared with the controller implemented in [20] along with ISMC and TSC. The controllers are implemented for various reference trajectories to ensure the efficacy of the control system designed.

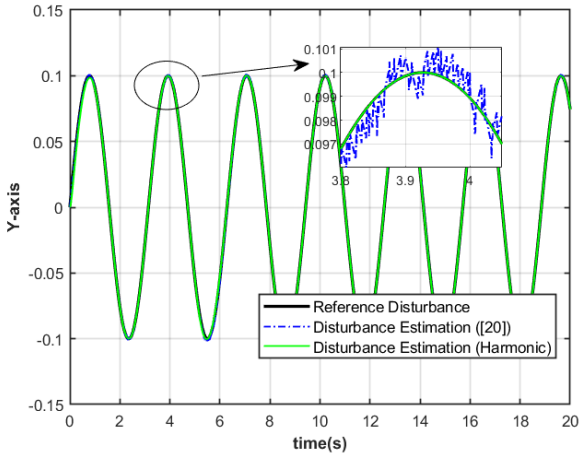

FIGURE 4. Y-axis disturbance estimation.

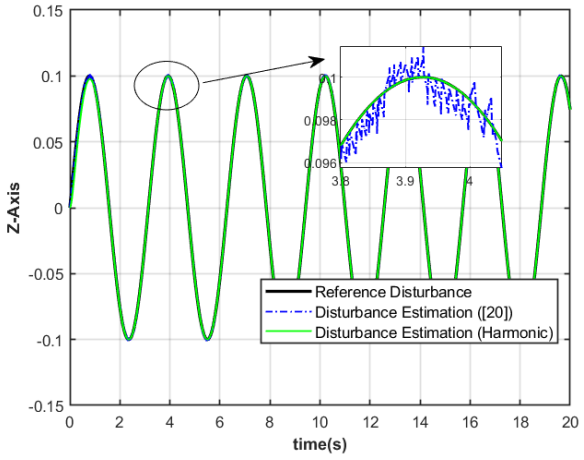

FIGURE 5. Z-axis disturbance estimation.

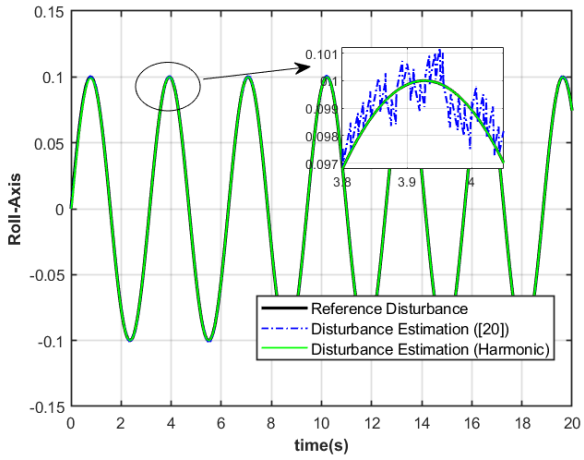

FIGURE 6. Roll-axis disturbance estimation.

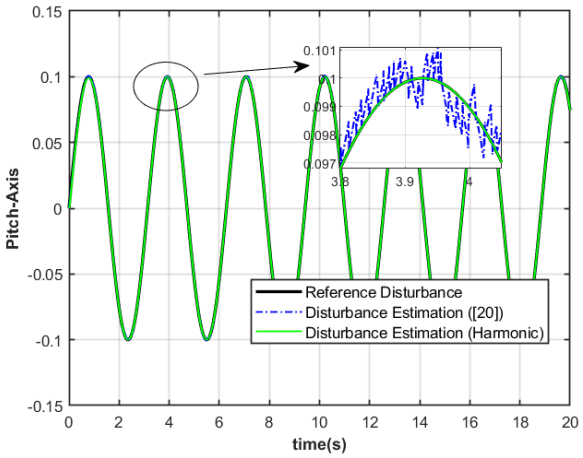

FIGURE 7. Pitch-axis disturbance estimation.

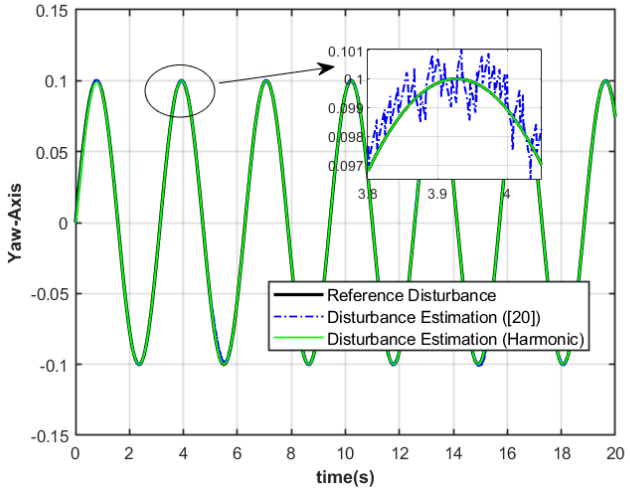

FIGURE 8. Yaw-axis disturbance estimation.

To analyse the performance of the controllers designed multiple performance indices would be used i.e. IAE (Integral Absolute Error), ITAE (Integral Time Absolute Error), ISE (Integral Square Error) and ITSE (Integral Time Square Error). The formulas for the performance index are as follows:

$$IAE = \int_0^t |e|\, dt$$
$$ITAE = \int_0^t |t\ e|\, dt$$
$$ISE = \int_0^t e^2 dt$$
$$ITSE = \int_0^t t\ e^2 dt \tag{53}$$

1) MULTI-STEP INPUT TRAJECTORY

For the design of multi-step input trajectory x^d and y^d are varied, while z and ψ are kept constant at $z^d = 2$ and $\psi^d = \pi/6$ respectively.

$$x^d = \begin{cases} 2, & 0 < t \leq 5 \\ 3, & 5 < t \leq 10 \\ 5, & t > 10 \end{cases}$$

$$y^d = \begin{cases} 1, & 0 < t \leq 5 \\ 2, & 5 < t \leq 10 \\ 4, & t > 10 \end{cases}$$

The results are depicted in the figures below:

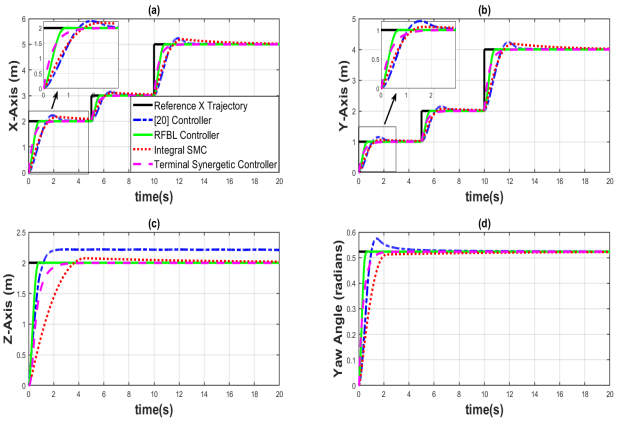

FIGURE 9. Multi-step input response for a) x-axis, b) y-axis, c) z-axis and d) ψ-axis.

While the control action for the multi-step input is shown in the following figure 10 and 11.

TABLE 1. Specification for X-axis (multi-input trajectory).

Controller Type	IAE	ITAE	ISE	ITSE
RFBL Controller	**1.81**	**9.47**	2.338	12.09
Controller in [20]	4.15	23.85	4.73	25.29
ISMC	4.561	30.82	3.933	21.06
TSC	1.927	10.56	**1.724**	**8.883**

TABLE 2. Specification for Y-axis (multi-input trajectory).

Controller Type	IAE	ITAE	ISE	ITSE
RFBL Controller	**1.368**	**9.34**	1.499	11.93
Controller in [20]	3.211	23.25	3.028	24.64
ISMC	3.405	28.76	2.522	20.87
TSC	1.54	10.34	**1.147**	**8.783**

TABLE 3. Specification for Z-axis (multi-input trajectory).

Controller Type	IAE	ITAE	ISE	ITSE	$t_s(sec)$
RFBL Controller	**0.6873**	**0.1493**	**0.975**	**0.1542**	**0.6985**
Controller in [20]	4.902	42.82	2.028	9.348	N/A
ISMC	3.515	9.564	3.609	2.749	11.3011
TSC	1.445	1.124	1.751	0.5289	2.3698

The results achieved by RFBL Controller as shown in table 1, 2, 3 and 4 outweigh all other controllers that have been

TABLE 4. Specification for Yaw(ψ)-axis (multi-input trajectory).

Controller Type	IAE	ITAE	ISE	ITSE	$t_s(sec)$
RFBL Controller	**0.1358**	**0.02216**	**0.05092**	**0.006052**	**0.5335**
Controller in [20]	0.3802	0.5432	0.1089	0.03055	3.5545
ISMC	0.5104	0.95	3.609	0.1422	3.0573
TSC	0.2041	0.1217	0.05415	0.009887	1.4737

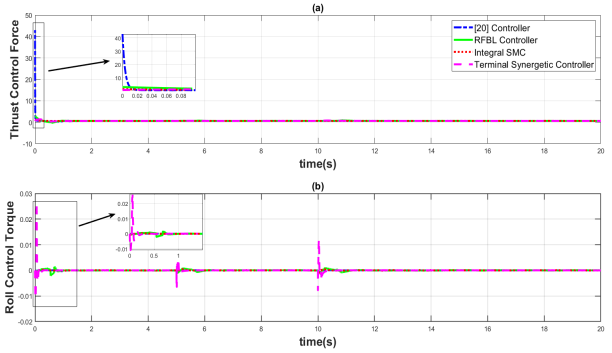

FIGURE 10. Control Input for multi-step input trajectory, a) Thrust Force, b) Roll Torque.

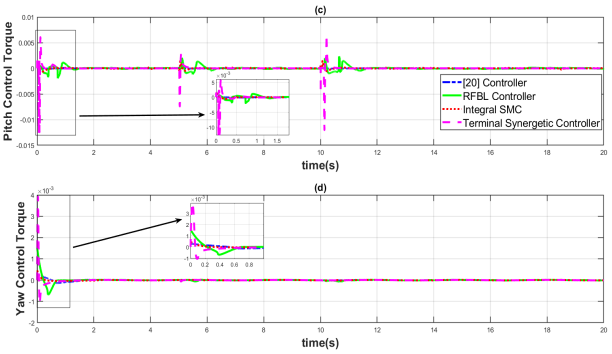

FIGURE 11. Control input for multi-step input trajectory, c) Pitch Torque, d) Yaw Torque.

compared. Even though TSC seems to outperform RFBL Controller in ISE and ITSE metrics as seen in table 1, however, there is a high spike in contents in the control effort of TSC as shown in figure 10 and 11.

2) CIRCULAR TRAJECTORY

To achieve a circular trajectory, an altitude of 1m to track the $z-axis$ is given, while the yaw angle ψ is kept at 0 rad. The desired trajectory to track for the x and y axis are: $x^d = \cos(0.5t)$ and $y^d = \cos(0.5t)$.

Figure 12 below shows the plot of circular trajectory.

The control action required to achieve the circular trajectory is depicted by the following figure 4 and 14:

All the tables 5, 6 and 7 show that RFBL Controller is far superior. The TSC once again shows high spikes therefore negating its effectiveness. The performance index depicts the RFBL Controller outperforming all the other controllers including that designed in [20].

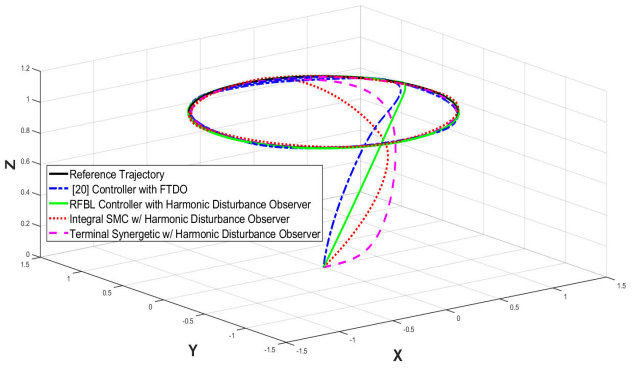

FIGURE 12. Circular trajectory plot.

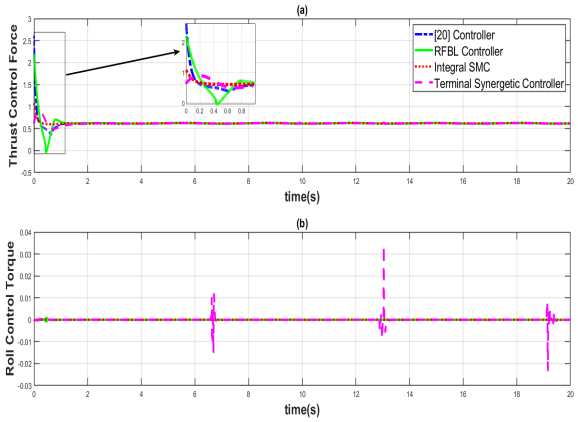

FIGURE 13. Control action for circular trajectory, a) Thrust Force, b) Roll Torque.

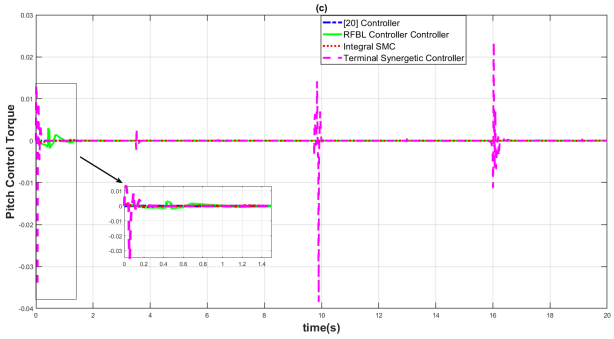

FIGURE 14. Control action for circular trajectory, c) Pitch Torque.

TABLE 5. Specification for X-axis (circular trajectory).

Controller Type	IAE	ITAE	ISE	ITSE
RFBL Controller	**1.045**	**7.353**	**0.2528**	**0.3782**
Controller in [20]	3.067	24.11	0.8191	3.61
ISMC	2.617	20.3	0.666	3.008
TSC	2.557	22.57	0.5141	3.291

3) 8/INFINITY SHAPED TRAJECTORY

Trajectory to attain shaped of numeric digit 8 or ∞ can be achieved by setting the desired commanded states as $x^d = \cos(0.5\,t)$, $y^d = \cos(0.5\,t)\sin(0.5\,t)$, $z^d = 1.5$ and $\psi^d = 0$.

TABLE 6. Specification for Y-axis (circular trajectory).

Controller Type	IAE	ITAE	ISE	ITSE
RFBL Controller	**0.7764**	**7.985**	**0.03748**	**0.3891**
Controller in [20]	2.567	26.09	0.3881	3.953
ISMC	2.134	22.42	0.3063	3.341
TSC	2.374	24.54	0.3474	3.693

TABLE 7. Specification for Z-axis (circular trajectory).

Controller Type	IAE	ITAE	ISE	ITSE	$t_s(sec)$
RFBL Controller	**0.2841**	**0.05047**	**0.2301**	**0.02649**	**0.5803**
Controller in [20]	0.5248	0.5584	0.2704	0.05723	2.2369
ISMC	1.179	1.609	0.6917	0.3686	2.6984
TSC	0.7498	0.5562	0.4857	0.1519	2.2203

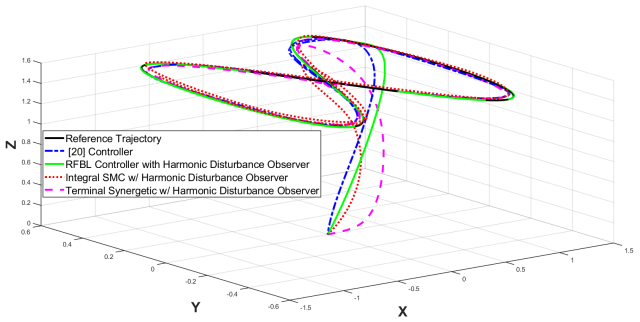

FIGURE 15. Plot of 8/infinity shaped trajectory.

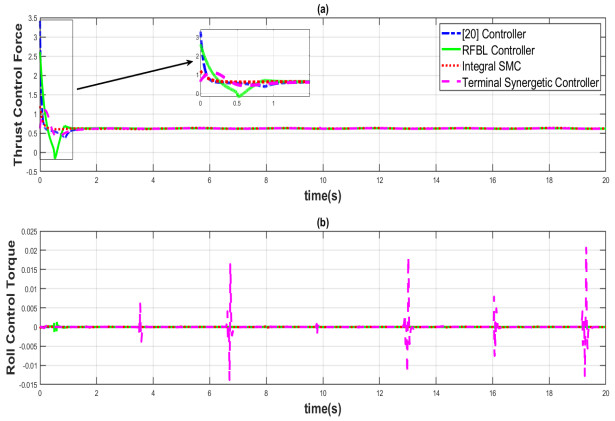

FIGURE 16. Control action for 8/infinity shaped trajectory, a) Thrust Force, b) Roll Torque.

TABLE 8. Specification for X-axis (infinity shaped trajectory).

Controller Type	IAE	ITAE	ISE	ITSE
RFBL Controller	**1.045**	**7.353**	**0.2528**	**0.3782**
Controller in [20]	3.067	24.11	0.8191	3.61
ISMC	2.617	20.3	0.666	3.008
TSC	2.557	22.57	0.5141	3.291

Results of tracking the infinity-shaped trajectory shown in table 8, 10 and 9 highlights the efficacy and superiority of the RFBL Controller over the compared controllers designed. All performance indices highlighted in bold show that the best results are achieved by the RFBL Controller.

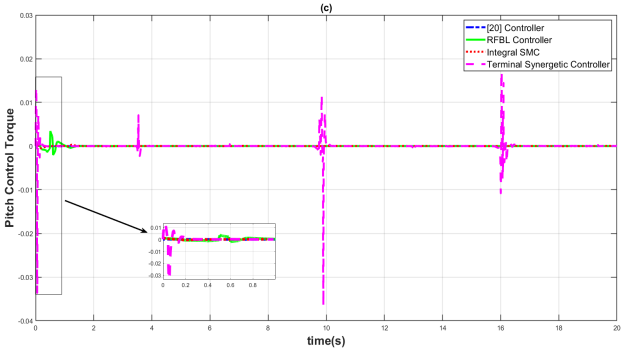

FIGURE 17. Control action for 8/infinity shaped trajectory, c) Pitch Torque.

TABLE 9. Specification for Y-axis (infinity shaped trajectory).

Controller Type	IAE	ITAE	ISE	ITSE
RFBL Controller	**0.837**	**8.528**	**0.04428**	**0.4544**
Controller in [20]	2.595	26.42	0.4137	4.244
ISMC	2.05	21.32	0.2722	2.903
TSC	2.274	23.49	0.3189	3.376

TABLE 10. Specification for Z-axis (infinity shaped trajectory).

Controller Type	IAE	ITAE	ISE	ITSE	$t_s(sec)$
RFBL Controller	**0.4759**	**0.09486**	**0.5083**	**0.07416**	**0.6443**
Controller in [20]	0.8686	0.7317	0.7347	0.1813	2.0092
ISMC	2.253	4.989	1.817	1.186	6.3582
TSC	1.099	0.8388	1.026	0.3128	2.3192

4) SQUARE TRAJECTORY

The commanded trajectory for this case is achieved by setting $z^d = 1.5$, $\psi^d = 0$. While x^d and y^d are set as:

$$x^d = \begin{cases} 0, & 0 < t \leq 2.5 \\ 2, & 2.5 < t \leq 10 \\ 0, & 10 < t \leq 15 \\ 2, & t > 15 \end{cases}$$

$$y^d = \begin{cases} 0, & 0 < t \leq 5 \\ 2, & 5 < t \leq 12.5 \\ 0, & t > 12.5 \end{cases}$$

TABLE 11. Specification for X-axis (square shaped trajectory).

Controller Type	IAE	ITAE	ISE	ITSE
RFBL Controller	2.246	21.1	3.165	29.49
Controller in [20]	5.094	50.18	6.458	61.55
ISMC	5.488	55.64	5.778	56.09
TSC	**2.184**	**20.43**	**2.197**	**19.95**

Only for the square trajectory tracking does the TSC achieve slightly better results compared to the RFBL Controller as shown in table 11 and 12 i.e. for the X and Y axis. However, RFBL Controller is way more superior in the Z axis as shown in table 13. The superiority of the TSC achieved in X and Y axis seems to be negated by the fact that

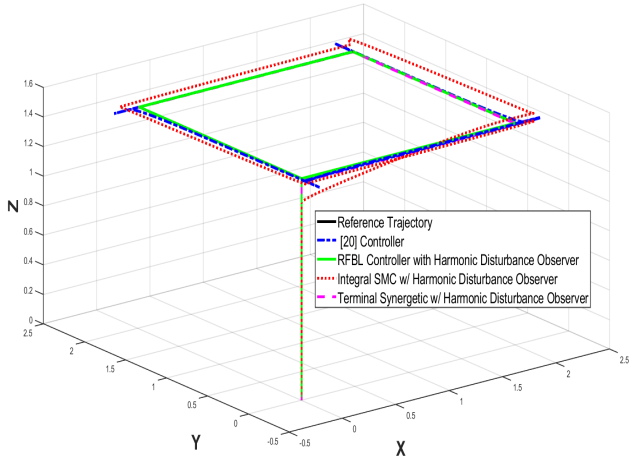

FIGURE 18. Plot of square shaped trajectory.

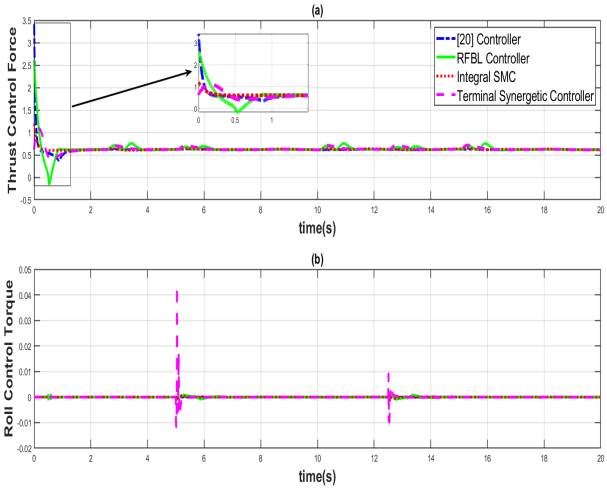

FIGURE 19. Control action for square shaped trajectory, a) Thrust Force, b) Roll Torque.

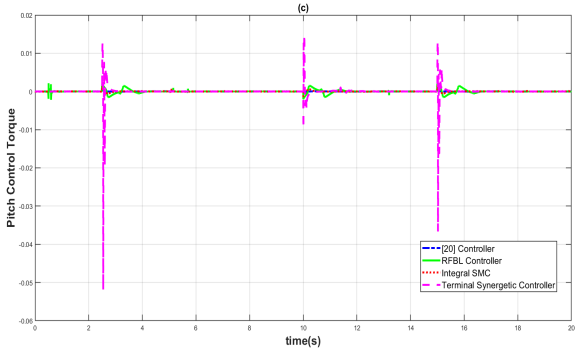

FIGURE 20. Control action for square shaped trajectory, c) Pitch Torque.

TABLE 12. Specification for Y-axis (square shaped trajectory).

Controller Type	IAE	ITAE	ISE	ITSE
RFBL Controller	1.481	13.31	2.069	18.46
Controller in [20]	3.375	32.01	4.214	38.46
ISMC	3.79	38.49	3.707	34.32
TSC	**1.462**	**13.11**	**1.492**	**13.24**

high spike content in its control effort can be seen in figure 8 and 20.

TABLE 13. Specification for Z-axis (square shaped trajectory).

Controller Type	IAE	ITAE	ISE	ITSE	$t_s(sec)$
RFBL Controller	**0.4759**	**0.09486**	**0.5083**	**0.07416**	**0.6443**
Controller in [20]	0.8686	0.7317	0.7347	0.1813	2.0092
ISMC	2.253	4.989	1.817	1.186	6.3582
TSC	1.099	0.8388	1.026	0.3128	2.3192

5) SPIRAL TRAJECTORY

To achieve a spiral trajectory, the yaw angle ψ is kept at 0 rad. The desired trajectory to track for the x, y and z axis are: $x^d = cos(0.5t)$, $y^d = cos(0.5t)$ and $z^d = t$.

Figure 21 shows the plot of the spiral trajectory.

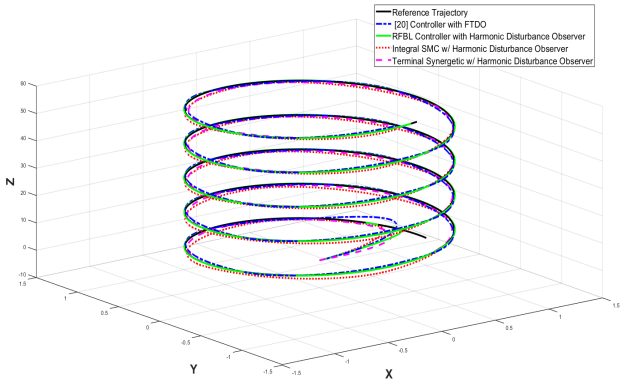

FIGURE 21. Spiral trajectory plot.

The control action required to achieve the spiral trajectory is depicted by figure 22 and 23:

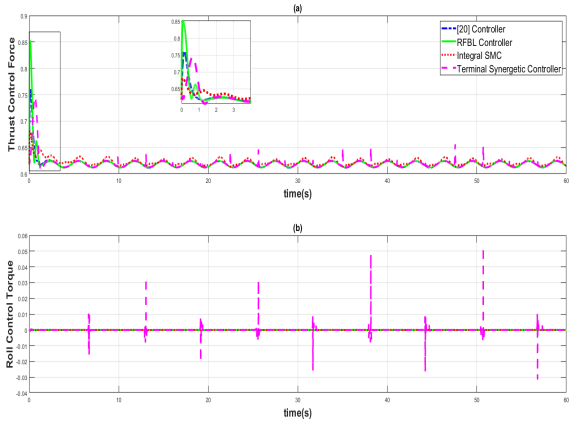

FIGURE 22. Control action for spiral trajectory, a) Thrust Force, b) Roll Torque.

Lastly, to test the efficacy of the RFBL Controller over other compared controllers, a spiral trajectory has been used. The results achieved by RFBL Controller outweigh all other controllers by a large extent as shown in table 14, 15 and 16. The X, Y and Z axis is tracked by the RFBL Controller with the highest accuracy, clearly depicted by the numbers highlighted in bold.

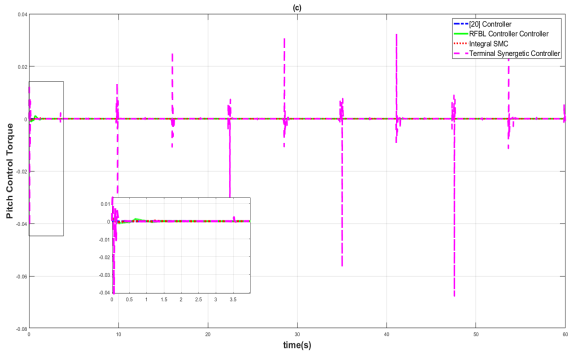

FIGURE 23. Control action for spiral trajectory, c) Pitch Torque.

TABLE 14. Specification for X-axis (spiral trajectory).

Controller Type	IAE	ITAE	ISE	ITSE
RFBL Controller	**2.655**	**71.45**	**0.3335**	**3.59**
Controller in [20]	8.182	227.6	1.581	33.86
ISMC	6.933	191.7	1.291	27.8
TSC	7.419	216.6	1.257	33.12

TABLE 15. Specification for Y-axis (spiral trajectory).

Controller Type	IAE	ITAE	ISE	ITSE
RFBL Controller	**2.253**	**67.21**	**0.1064**	**3.164**
Controller in [20]	7.551	226.2	1.117	33.28
ISMC	6.319	190.8	0.9072	27.64
TSC	7.101	214.4	1.056	32.26

TABLE 16. Specification for Z-axis (spiral trajectory).

Controller Type	IAE	ITAE	ISE	ITSE
RFBL Controller	**6.117**	**180.2**	**0.6286**	**18.04**
Controller in [20]	19.83	592.8	6.571	195.3
ISMC	74.87	2061	98.12	2422
TSC	40.45	1232	27.38	843.3

C. HARDWARE IN LOOP VALIDATION

To emulate our controller and plant in a real setting, a Hardware-in-Loop (HIL) experiment is carried out. Although implementation on real hardware provides a better validation, due to limited resources S-HIL was implemented. S-HIL approximates the controller in a real-time setting and provides a cost-effective solution by implementing both the plant and controller on a microprocessor field-programmable gate array (FPGA).

S-HIL (Single Hardware in Loop) is implemented by discretization of the continuous time blocks in Simulink/Matlab with appropriate sample time [33]. The implementation for S-HIL is carried out on MicroLabBox dSPACE RTI-1202 platform. The results shown in Fig. 24 show good tracking of S-HIL results in comparison with simulation. A low computational burden was seen during implementation in S-HIL environment since both each disturbance observer is a two-state ordinary differential equation and can be easily solved using a discrete-time solver.

The control efforts seen in Fig. 25 vary slightly initially during the transient phase. After the transition phase, the control efforts for both the S-HIL and simulation seem to be tracked closely. Hardware in Loop (HIL) provides results that are safe for future practical implementation.

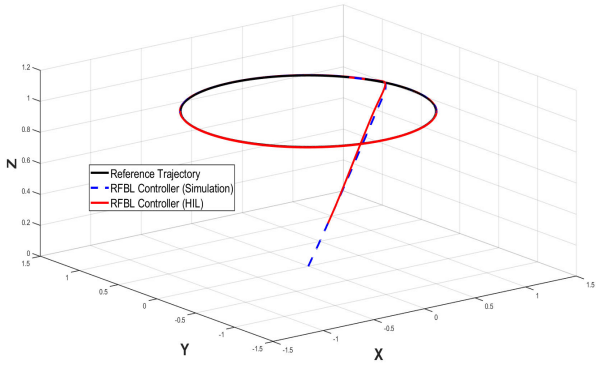

FIGURE 24. Comparison of S-HIL and simulation of RFBL controller for the circular trajectory.

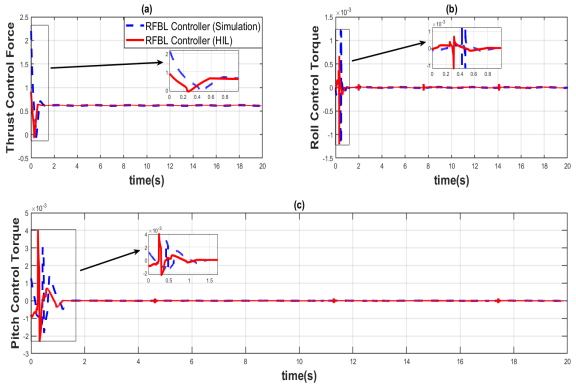

FIGURE 25. Comparison of S-HIL and simulation of RFBL control efforts a) Thrust Control Force, b) Roll Control Torque, c) Pitch Control Torque.

TABLE 17. Quadrotor drone parameters.

Parrot Mambo Drone Parameters		
Parameter Name	Value	Units
Mass, m	0.063	kg
Arm lenth, l	0.062	m
Moment of Inertia along x-axis, I_x	5.8286×10^{-5}	kg.m^2
Moment of Inertia along y-axis, I_y	7.1691×10^{-5}	kg.m^2
Moment of Inertia along z-axis, I_z	1×10^{-4}	kg.m^2
Thrust Coefficient, k_F	0.01	N/(rad$^2/s^2$)
Thrust Coefficient, k_M	7.8263×10^{-4}	Nm/(rad$^2/s^2$)
Aerodynamic Coefficients, ξ_z , ξ_ϕ, ξ_θ, ξ_ψ,ξ_x, ξ_y	0.075	N.s/rad

V. CONCLUSION

The results verify that the RFBL Controller achieves superior performance compared to the other implemented controllers. The TSC may seem to outperform RFBL Controller in a few cases, however, the high spikes in control action observed

TABLE 18. Robust Feedback Linearization (RFBL) controller parameters.

Controller Parameters	
Parameter	Value
$K_{pz}, K_{p\phi}, K_{p\theta}, K_{p\psi}, K_{px}, K_{py}$	3
$K_{dz}, K_{d\phi}, K_{d\theta}, K_{d\psi}, K_{dx}, K_{dy}$	6
k_{1z}	7
$k_{1\phi}$	4
$k_{1\theta}, k_{1\psi}, k_{1x}, k_{1y}$	6
$k_{2\phi}$	1.1
$k_{2z}, k_{2\theta}, k_{2\psi}$	1
k_{2x}	0.5
k_{2x}	0.6
$c_1, c_2, c_3, c_4, c_5, c_6$	10

TABLE 19. Integral sliding mode controller (ISMC) parameters.

Controller Parameters	
Parameter	Value
$k_z, k_{px}, k_{py}, k_{p\psi}$	2
k_ϕ, k_θ	4
$c_{1z}, c_{1\theta}, c_{1\psi}, c_{1x}, c_{1y}$	10
$c_{1\psi}$	8
$c_{2z}, c_{2\psi}$	1
$c_{2\theta}, c_{2\psi}, c_{2x}, c_{2y}$	3

TABLE 20. Terminal synergetic controller (TSC) parameters.

Controller Parameters	
Parameter	Value
w_{1z}	10
2_{2z}	5
$w_{1\phi}, w_{1\theta}, w_{1\psi}, w_{1x}, w_{1y}$	1000
$w_{2\phi}, w_{2\theta}, w_{2\psi}, w_{2x}, w_{2y}$	200
T_z ,$T_\phi, T_\theta, T_\psi, T_x, T_y$	1000
p_1, p_2	5
q_1, q_2	3

in the control effort negate the response it achieves by causing actuator saturation. Lower error tracking and fast settling times are noticeable for RFBL Controller in addition to robustness to external disturbances. Also, the nonlinear harmonic disturbance observer achieves a better estimation of disturbances and tracks the reference disturbances much more precisely as compared to the finite time disturbance observer. Hardware-in-Loop provides validation of the controller for practical implementation.

In the future, the controllers will be implemented on the experimental drone platform for further validation of results in real-time. Moreover, various other published controllers and their associated disturbance observers will be included for the comparison analysis, benefiting the readers. Additionally, controller parameters can be selected by using meta-heuristics algorithms by having an appropriate objective function. Another area that needs to be explored is disturbance observer for mismatched disturbances.

CONFLICT OF INTEREST STATEMENT

The authors declare that there is no conflict of interest.

APPENDIX

See Tables 17–20.

REFERENCES

[1] J. Koetsier. (Apr. 2022). *Drone Delivery is Live Today, and it's 90% Cheaper Than Car-Based Services*. [Online]. Available: https://www.forbes.com/sites/johnkoetsier/2021/08/18/drone-delivery-is-live-today-and-its-90-cheaper-than-car-based-services/

[2] L. D. P. Pugliese, F. Guerriero, and G. Macrina, "Using drones for parcels delivery process," *Proc. Manuf.*, vol. 42, pp. 488–497, Dec. 2020.

[3] A. Farooq, S. Shafi, Z. Ullah, M. Quresh, and N. Chumuang, "A lightweight controller for autonomous following of a target platform for drones," in *Proc. IEEE Int. Conf. Cybern. Innov. (ICCI)*, Mar. 2023, pp. 1–6.

[4] T. P. Nascimento and M. Saska, "Position and attitude control of multi-rotor aerial vehicles: A survey," *Annu. Rev. Control*, vol. 48, pp. 129–146, Apr. 2019.

[5] N. Ahmed and M. Chen, "Sliding mode control for quadrotor with disturbance observer," *Adv. Mech. Eng.*, vol. 10, no. 7, Jul. 2018, Art. no. 168781401878233.

[6] N. Ahmed, A. Raza, S. A. A. Shah, and R. Khan, "Robust composite-disturbance observer based flight control of quadrotor attitude," *J. Intell. Robotic Syst.*, vol. 103, no. 1, P. 11, Sep. 2021.

[7] N. Ahmed, M. Chen, and S. Shao, "Disturbance observer based tracking control of quadrotor with high-order disturbances," *IEEE Access*, vol. 8, pp. 8300–8313, 2020.

[8] H. Maqsood and Y. Qu, "Nonlinear disturbance observer based sliding mode control of quadrotor helicopter," *J. Electr. Eng. Technol.*, vol. 15, no. 3, pp. 1453–1461, May 2020.

[9] H. L. N. N. Thanh, C. H. Lee, N. X. Mung, and S. K. Hong, "An effective dynamic sliding mode control based nonlinear disturbance observer for a quadrotor UAV," in *Proc. IEEE 16th Int. Conf. Control Autom. (ICCA)*, Oct. 2020, pp. 1553–1558.

[10] L. Cui, X. Hou, Z. Zuo, and H. Yang, "An adaptive fast super-twisting disturbance observer-based dual closed-loop attitude control with fixed-time convergence for UAV," *J. Franklin Inst.*, vol. 359, no. 6, pp. 2514–2540, Apr. 2022.

[11] B. Wang, X. Yu, L. Mu, and Y. Zhang, "Disturbance observer-based adaptive fault-tolerant control for a quadrotor helicopter subject to parametric uncertainties and external disturbances," *Mech. Syst. Signal Process.*, vol. 120, pp. 727–743, Apr. 2019.

[12] A. Castillo, R. Sanz, P. Garcia, W. Qiu, H. Wang, and C. Xu, "Disturbance observer-based quadrotor attitude tracking control for aggressive maneuvers," *Control Eng. Pract.*, vol. 82, pp. 14–23, Jan. 2019.

[13] S. Mishra, T. Rakstad, and W. Zhang, "Robust attitude control for quadrotors based on parameter optimization of a nonlinear disturbance observer," *J. Dyn. Syst., Meas., Control*, vol. 141, no. 8, Aug. 2019, Art. no. 081003.

[14] J. Dávila and S. Salazar, "Robust control of an uncertain UAV via high-order sliding mode compensation," *IFAC-PapersOnLine*, vol. 50, no. 1, pp. 11553–11558, Jul. 2017.

[15] D. Shi, Z. Wu, and W. Chou, "Super-twisting extended state observer and sliding mode controller for quadrotor UAV attitude system in presence of wind gust and actuator faults," *Electronics*, vol. 7, no. 8, p. 128, Jul. 2018.

[16] C.-C. Hua, K. Wang, J.-N. Chen, and X. You, "Tracking differentiator and extended state observer-based nonsingular fast terminal sliding mode attitude control for a quadrotor," *Nonlinear Dyn.*, vol. 94, no. 1, pp. 343–354, Oct. 2018.

[17] H. Rios, R. Falcon, O. A. Gonzalez, and A. Dzul, "Continuous sliding-mode control strategies for quadrotor robust tracking: Real-time application," *IEEE Trans. Ind. Electron.*, vol. 66, no. 2, pp. 1264–1272, Feb. 2019.

[18] S. W. Ha and B. S. Park, "Disturbance observer-based control for trajectory tracking of a quadrotor," *Electronics*, vol. 9, no. 10, p. 1624, Oct. 2020.

[19] A. Aboudonia, A. El-Badawy, and R. Rashad, "Disturbance observer-based feedback linearization control of an unmanned quadrotor helicopter," *Proc. Inst. Mech. Eng., I, J. Syst. Control Eng.*, vol. 230, no. 9, pp. 877–891, Oct. 2016.

[20] V. K. Tripathi, A. K. Kamath, L. Behera, N. K. Verma, and S. Nahavandi, "Finite-time super twisting sliding mode controller based on higher-order sliding mode observer for real-time trajectory tracking of a quadrotor," *IET Control Theory Appl.*, vol. 14, no. 16, pp. 2359–2371, Nov. 2020.

[21] A. Moeini, A. F. Lynch, and Q. Zhao, "Disturbance observer-based nonlinear control of a quadrotor UAV," *Adv. Control Appl., Eng. Ind. Syst.*, vol. 2, no. 1, p. e24, 2020.

[22] M. Sharma and I. Kar, "Finite time disturbance observer based geometric control of quadrotors," *IFAC-PapersOnLine*, vol. 53, no. 1, pp. 295–300, 2020.
[23] B. Tian, H. Lu, Z. Zuo, Q. Zong, and Y. Zhang, "Multivariable finite-time output feedback trajectory tracking control of quadrotor helicopters," *Int. J. Robust Nonlinear Control*, vol. 28, no. 1, pp. 281–295, Jan. 2018.
[24] O. Mechali, L. Xu, Y. Huang, M. Shi, and X. Xie, "Observer-based fixed-time continuous nonsingular terminal sliding mode control of quadrotor aircraft under uncertainties and disturbances for robust trajectory tracking: Theory and experiment," *Control Eng. Pract.*, vol. 111, Jun. 2021, Art. no. 104806.
[25] H. Hamadi, B. Lussier, I. Fantoni, C. Francis, and H. Shraim, "Observer-based super twisting controller robust to wind perturbation for multirotor UAV," in *Proc. Int. Conf. Unmanned Aircr. Syst. (ICUAS)*, Jun. 2019, pp. 397–405.
[26] L. Besnard, Y. B. Shtessel, and B. Landrum, "Quadrotor vehicle control via sliding mode controller driven by sliding mode disturbance observer," *J. Franklin Inst.*, vol. 349, no. 2, pp. 658–684, Mar. 2012.
[27] D. D. Dhadekar, P. D. Sanghani, K. K. Mangrulkar, and S. E. Talole, "Robust control of quadrotor using uncertainty and disturbance estimation," *J. Intell. Robotic Syst.*, vol. 101, no. 3, pp. 1–21, Mar. 2021.
[28] Y. Song, L. He, D. Zhang, J. Qian, and J. Fu, "Neuroadaptive fault-tolerant control of quadrotor UAVs: A more affordable solution," *IEEE Trans. Neural Netw. Learn. Syst.*, vol. 30, no. 7, pp. 1975–1983, Jul. 2019.
[29] J. A. Moreno, "Lyapunov approach for analysis and design of second order sliding mode algorithms," in *Sliding Modes After 1st Decade 21st Century*. Cham, Switzerland: Springer, 2011, pp. 113–149.
[30] S. Li, J. Yang, W.-H. Chen, and X. Chen, *Disturbance Observer-Based Control: Methods and Applications*. Boca Raton, FL, USA: CRC Press, 2014.
[31] Y. Pan, C. Yang, L. Pan, and H. Yu, "Integral sliding mode control: Performance, modification, and improvement," *IEEE Trans. Ind. Informat.*, vol. 14, no. 7, pp. 3087–3096, Jul. 2018.
[32] A. Kolesnikov et al., *Modern Applied Control Theory: Synergetic Approach in Control Theory*, vol. 2. Moscow, Russia: TSURE Press (in Russia), 2000.
[33] A. Rosa, M. Silva, M. Campos, R. Santana, W. Rodrigues, L. Morais, and S. I. Seleme, Jr., "SHIL and DHIL simulations of nonlinear control methods applied for power converters using embedded systems," *Electronics*, vol. 7, no. 10, p. 241, Oct. 2018.

MOHAMMAD SADIQ received the master's degree in control engineering from the National University of Sciences and Technology (NUST), Pakistan, and the master's degree in engineering design from KTH, Sweden. His current research interests include nonlinear control, mechatronics system design, and disturbance observers.

RAMEEZ HAYAT received the Ph.D. degree in robotics from the Technical University of Munich, Germany. He has worked on design, fabrication, and control of 3 and 7-Degree-of-Freedom robot manipulators. His research involved the modeling of kinematics of the robotic manipulators and design of model-free adaptive controller robust to modeling uncertainties and disturbances. More recently, he is working on extending the ideas of model-free robust adaptive control to safety guarantees of robotic manipulators in the context of human robot interactions. Some of his other interests include smart-grids and renewable energy systems in the context of climate-change which can benefit from the control design ideas.

KAMRAN ZEB received the B.Sc.E.E. and M.Sc.E.E. degrees from the COMSATS Institute of Information and Technology, Abbottabad, Pakistan, in 2013 and 2016, respectively, and the Ph.D. degree from Pusan National University, Busan, South Korea. He is currently an Assistant Professor (on leave for Postdoctoral with the King Fahd University of Petroleum and Minerals) with the Department of Electrical Engineering, School of Electrical Engineering and Computer Science, National University of Sciences and Technology, Islamabad, Pakistan for the last three years. He served the University of Management and Technology, Lahore, Pakistan for one and half year as a Lecturer. His research interests include power converters, control systems, renewable energies, electric vehicles, robotics, modular multilevel inverter, and electrical drive. He has contributed 70 papers in various reputed journals and conferences with more than 2100 citations and H-index 22 and H-index 39.

AHMED AL-DURRA (Senior Member, IEEE) received the B.Sc., M.Sc., and Ph.D. degrees (summa cum laude) in ECE from The Ohio State University, in 2005, 2007, and 2010, respectively.

He joined the Electrical Engineering Department, Petroleum Institute (PI), United Arab Emirates, as an Assistant Professor, in 2010. He was promoted to an Associate Professor, in 2015. Since 2020, he has been a Professor with the Electrical Engineering and Computer Science Department, Khalifa University, United Arab Emirates, where he is currently an Associate Provost for Research. His research interests include the applications of control and estimation theory on power systems stability, micro and smart grids, renewable energy systems and integration, and process control. He has accomplished and he has been working on several research projects at international and national levels (exceeding 25M USD). He is the Head of the Energy Systems, Control and Optimization Laboratory, ADRIC and the Industry Engagement Theme Lead for the Advanced Power and Energy Center. He has one U.S. patent, one edited book, 12 book chapters, and over 280 scientific articles in top-tier journals and refereed international conference proceedings. He has supervised/co-supervised over 30 Ph.D./Master students. He is an Editor of IEEE TRANSACTIONS ON SUSTAINABLE ENERGY and IEEE POWER ENGINEERING LETTERS, and an Associate Editor of IEEE TRANSACTIONS ON INDUSTRY APPLICATIONS, *IET Renewable Power Generation*, and *IET Generation Transmission and Distribution*. In 2014, he obtained the PI Research and Scholarship Award for Junior Faculty, and he was elevated to the grade of IEEE Senior Member. He was awarded the United Arab Emirates Pioneers Award—United Arab Emirates Scientists, in 2018. He was the Winner of the prestigious Khalifa Award for Education—Distinguished University Professor in Scientific Research, from 2018 to 2019. He was awarded the Faculty Research Excellence Award-Khalifa University, in 2020.

ZAHID ULLAH (Graduate Student Member, IEEE) received the B.S. degree in electrical engineering from UET Peshawar, in 2014, and the M.S. degree in electrical engineering from COMSATS University Islamabad, Abbottabad Campus, Abbottabad, Pakistan, in 2017. He is currently pursuing the Ph.D. degree in electrical engineering with Politecnico di Milano, Italy. He was a Lecturer with UMT Lahore, Pakistan, from 2017 to 2020. He has published various papers in reputed journals and IEEE conference proceedings. His research interests include smart grid, energy management, renewable energy systems, ICTs for power systems, V2G, and machine and deep learning.

Open Access funding provided by 'Politecnico di Milano' within the CRUI CARE Agreement